All-fiber, high-average-power nanosecond laser based on core-diameter adjustment

Songtao Du (杜松涛)[1*], Ziwei Wang (王子薇)[1,2], Zhaokun Wang (王兆坤)[1,2], Jing He (何 晶)[1,2], Jun Zhou (周 军)[1], and Qihong Lou (楼祺洪)[1]

[1] *Shanghai Institute of Optics and Fine Mechanics, Chinese Academy of Sciences, Shanghai 201800, China*

[2] *University of Chinese Academy of Sciences, Beijing 100049, China*

[*] *Corresponding author: songtaodu@mail.siom.ac.cn*

Received May 2, 2013; accepted May 31, 2013; posted online August 28, 2013

Core-diameter adjustment, in analogy to doping management, is proposed in this letter for balancing thermal load and nonlinear effects. In this scheme, the core-to-cladding ratio increases with increasing core diameter along the direction of signal and pump propagation. An all-fiber-integrated Yb-doped master oscillator power amplification (MOPA) is successfully demonstrated. Two segments of fiber with different core diameters but same inner-cladding diameters and doping levels are spliced together and used as gain fibers in the last stage. A maximum average output power of 200 W at an overall slope efficiency of 71% is achieved from the MOPA with a pulse energy of 2 mJ and peak power as high as 80 kW.

OCIS codes: 140.3280, 140.3510, 140.3615.

doi: 10.3788/COL201311.091402.

Pulsed fiber master oscillator power amplification (MOPA) is receiving increasing attention over the past decade because of its potential advantages, such as efficiency, compactness, reliability, ease of thermal management, and high average power levels. Using high-power or high-energy fiber amplifiers, nanosecond fiber lasers reach above 100-W average power[1−3] or several millijoules per pulse[4−6]. However, a well-known trade-off exists between minimizing thermal effects and nonlinear effects, which limits the average and peak powers, respectively. In general, nonlinear effects scale with the intensity in the fiber core and the propagation length. Hence, their thresholds can be pushed by using low-nonlinearity fibers possessing a large core and short absorption length[7−11]. Recently, high-power fiber amplifiers based on rod-like photonic crystal fibers have been spectrally combined up to an average power of 1.1 kW[12]. These sources rely on photonic crystal technology, but these gain media are rigid and mostly rely on free-space beam propagation. Thermal effects are also not considered. To balance thermal load and nonlinear effects, Elahi *et al.* proposed doping management[13], which involved varying doping level gain fibers, and demonstrated a 100-W, 4.5-ps, 100-MHz, all-fiber-integrated amplifier using discrete doping management, which was implemented by combining fibers of low-doped and a high-doped Yb fibers.

However, the absorption of pump power is generally constrained not only by doping density but also by core-to-cladding ratios[13]. We propose core-diameter adjustment, in analogy to doping management, to balance thermal load and nonlinear effects. In this scheme, the core-to-cladding ratio increases with increasing core diameter along the direction of signal and pump propagation for forward pumping. Initially, the signal power is at a minimum and the pump is at a maximum. Starting with a lower core-to-cladding ratio ensures that the pump absorption is lower and the thermal load is reduced, which is the same as in doping management. Moreover, the smallest core diameter maintains the highest density of signal power in the core, which increases the amplification efficiency. With decreased pump power and increased signal power, the core-to-cladding ratio increases to minimize the gain length and consequently minimize the nonlinear effects. An increase in core diameter can further decrease nonlinear effects. Two segments of fiber with different core diameters but same inner-cladding diameters and doping levels are spliced together and used as gain fibers in the last stage of the laser system. The laser generated 200 W at 100 kHz with a pulse duration of 25 ns from an all-fiber-integrated amplifier.

Figure 1 shows a schematic diagram of the experimental setup. The amplifier consists of two gain stages. The seed laser is a directly modulated diode with a fiber-cascaded amplification system (Keopsys Inc., France). In the experiment, the seed laser can provide a maximum of 2-W average power of a 1 064-nm pulse with a pulse duration of 25 ns and adjustable repetition frequency of 50–150 kHz. The seed laser output is coupled into the first amplifier stage via an in-line optical

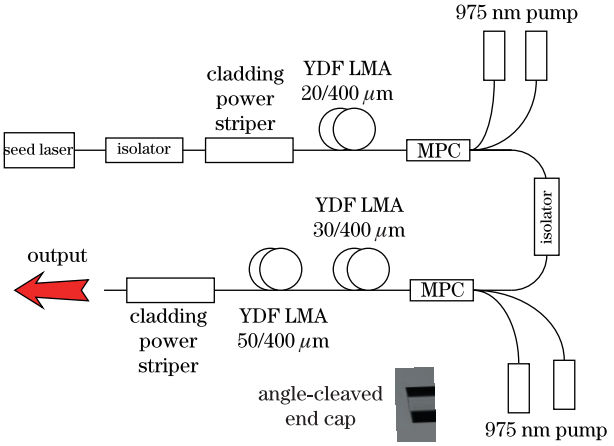

Fig. 1. Schematic diagram of the experimental setup. Inset: angle-cleaved end cap. YDF: Yb-doped fiber; LMA: large mode area.

Fig. 2. Micrograph of a good fusion splice.

isolator. The gain medium of the first-stage amplifier is a double-cladding (DC) Yb 20/400 μm fiber with a core and inner-cladding NAs of 0.06 and 0.45, respectively. The fiber is backward-pumped by two 975-nm fiber-pigtailed diode lasers, each laser can provide 25-W pump power, through a $(6 + 1) \times 1$ combiner. The maximum saturated output power from this stage is 15 W with a repetition rate of 100 kHz, while the pulse energy is 150 μJ. The pulse duration is maintained at 25 ns at this stage.

The output of the first stage is coupled into the signal fiber of a $(6 + 1) \times 1$ combiner via an in-line high-power optical isolator. The coupling efficiency is approximately 85%. The power amplifier is a hybrid gain fiber composed of a DC Yb 30/400 μm fiber and a DC Yb 50/400 μm fiber. The DC Yb 30/400 μm fiber is 3-m long with 3-dB/m absorption at 976 nm, and the DC Yb 50/400 μm fiber is 2.5-m long with 5.5-dB/m absorption at 976 nm. Both fibers have the same core and inner-cladding NA, which enable very low-loss splicing between them. Using asymmetrically-fattened splice[14] and symmetrically-tapered splice[15], the splice loss between DC Yb 30/400 μm fiber and DC Yb 50/400 μm fiber is reduced to 0.05 dB. Figure 2 shows a micrograph of a good fusion splice completed by a Vytran splicer. Six fiber-coupled pump diodes are used as pump sources. Each of these diodes provides 50 W of pump power at the central wavelength of 976 nm. In case of any damage to the output end, a 1.7-mm-long pure silica fiber end-cap is spliced to the fiber to reduce the power density of the amplifier fiber. The end-cap is cut into a slope of 8° to eliminate the amplified spontaneous emission (ASE) and self-oscillation effect, as shown in the inset of Fig. 1. This all-fiber-integrated amplifier has efficient pump power conversion as well as a compact and steady structure.

The amplification of the hybrid gain fibers (named fiber A) is compared with a 4-m-long DC Yb 50/400 μm fiber (named fiber B), which is used in the final stage instead. Figure 3 shows the measured power scaling behaviors of these two kinds of fiber. The output power of fiber B is lower than that of fiber A. This result is attributed to the strong gain saturation at the beginning of fiber B, where the signal power is lowest and the pump is highest. Gain saturation is weak at the beginning of fiber A because of the highest density of signal power in the core and the lower pump absorption. Fiber B is damaged by thermal effect when pump power exceeds 200 W. The surface temperature of the gain fiber is measured with a thermal infrared imager (NEC TH9100WRI) under the same fiber cooling conditions when pump power is 150 W. The temperature distribution along fiber A is essentially uniform. The highest temperature is only 58 °C, which is located at the splice point between the DC Yb 30/400 μm fiber and the DC Yb 50/400 μm fiber. The temperature distribution obviously varies along fiber B and approximately decays exponentially. The highest temperature is 92 °C and the high-temperature region is mainly focused on the first 1 m because of the high absorption of pump power. This thermal effect is a great challenge for fiber cooling.

Finally, using hybrid gain fiber, a maximum average output power of 200 W is obtained at a launched pump power of 275 W with a slope efficiency of 71%, as plotted in Fig. 3. The laser power linearly increases with the pump power and shows no evidence of roll-over even at the highest output power. The maximum output power is limited to the available pump power. The surface temperature of the gain fiber is also measured. The highest temperature of the gain fiber is maintained below 65 °C at maximum output. Figure 4 shows the spectra of the pulses at maximum output power. The spectral bandwidth increases because of self-phase modulation (SPM), as discussed in Refs. [16,17]. However, no signs of stimulated Raman scattering (SRS) and ASE are observed even when the MOPA is running at an output power of 200 W. Figure 5 shows the comparison of pulse shapes with seed source when the output power reaches 100 and 200 W, respectively. The leading edge of the output pulses increases with increasing output power. These results are due to the fact that the gain of the pulse rise edge is often higher than the gain of the pulse fall edge in a fiber MOPA system. Pulse distortion is observed at the maximum output power because of SPM.

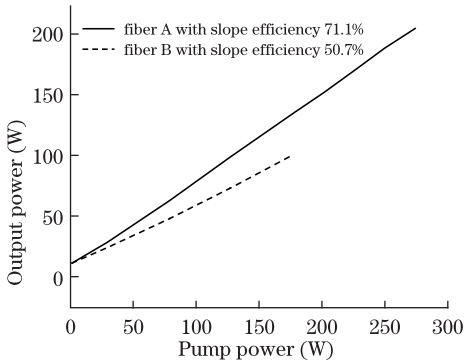

Fig. 3. Output power versus pump power of the two kinds of gain fibers.

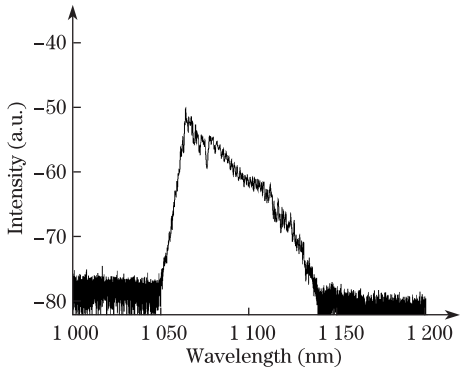

Fig. 4. Spectrum of the output.

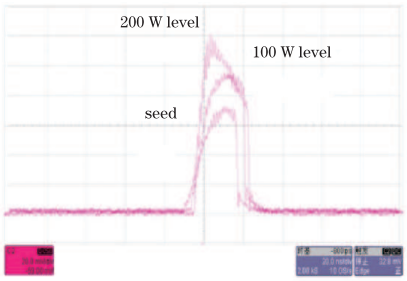

Fig. 5. Pulse shape of seed and output pulse at 100 and 200 W.

In conclusion, an all-fiber-integrated Yb-doped MOPA is successfully demonstrated. In this laser, two segments of fiber with different core diameters but with the same inner-cladding diameters and doping levels are spliced together and used as gain fibers in the last stage. This scheme is referred to as core diameter adjustment, which serves to minimize thermal load and nonlinear effects. The constructed laser system achieves a maximum average output power of 200 W at an overall slope efficiency of 71%. This system has a pulse energy of 2 mJ and peak power as high as 80 kW. Such a high-average-power and high repetition-rate nanosecond-pulsed laser with considerable pulse energies is desirable for many industrial high-speed material processing applications such as cutting, welding, and drilling.

References

1. A. Liu, M. A. Norsen, and R. D. Mead, Opt. Lett. **30,** 67 (2005).
2. W. Li, Q. Hao, M. Yan, and H. Zeng, Opt. Express **17,** 10113 (2009).
3. S. Du, X. Liu, J. Zhou, Y. Xue, B. He, J. Dong, Y. Wei, Q. Lou, Z. Yuan, and W. Wang, Opt. Eng. **49,** 024201 (2010).
4. D. Lin, S. Alam, K. Chen, A. Malinowski, S. Norman, and D. Richardson, in *Proceedings of CLEO/IQEC 2009* CFM4 (2009).
5. Z. Yang, X. Hu, Y. Wang, W. Zhang, and W. Zhao, Chin. Opt. Lett. **9,** 041401 (2011)
6. R. Zhou, Y. Ju, Y. Zhang, and Y. Wang, Chin. Opt. Lett. **9,** 071401 (2011).
7. J. Limpert, O. Schmidt, J. Rothhardt, F. Röser, T. Schreiber, A. Tünnermann, S. Ermeneux, P. Yvernault, and F. Salin, Opt. Express **14,** 2715 (2006).
8. O. Schmidt, J. Rothhardt, T. Eidam, F. Röser, J. Limpert, A. Tünnermann, K. P. Hansen, C. Jakobsen, and J. Broeng, Opt. Express **16,** 3918 (2008).
9. F. Röser, T. Eidam, J. Rothhardt, O. Schmidt, D. N. Schimpf, J. Limpert, and A. Tünnermann, Opt. Lett. **32,** 3495 (2007).
10. D. Brooks and F. Di Teodoro, Appl. Phys. Lett. **89,** 111119 (2006).
11. O. Schmidt, J. Rothhardt, F. Röser, S. Linke, T. Schreiber, K. Rademaker, J. Limpert, A. Tünnermann, S. Ermeneux, P. Yvernault, and F. Salin, Opt. Lett. **31,** 1551 (2007).
12. O. Schmidt, C. Wirth, I. Tsybin, T. Schreiber, R. Eberhardt, J. Limpert, and A. Tünnermann, Opt. Lett. **34,** 1567 (2009).
13. P. Elahi, S. Yılmaz, Ö. Akçaalan, H. Kalaycıoğlu, B. Öktem, C. Senel, F. Ö. Ilday, and K. Eken, Opt. Lett. **37,** 3042 (2012).
14. E. M. O'Brien and C. D. Hussey, Electron. Lett. **35,** 168 (1999).
15. A. Ishikura, Y. Kato, and M. Miyauchi, Appl. Opt. **25,** 3460 (1986).
16. P. Dupriez, A. Piper, A. Malinowski, J. K. Sahu, M. Ibsen, B. C. Thomsen, Y. Jeong, L. M. B. Hickey, M. N. Zervas, J. Nilsson, and D. J. Richardson, Photon. Technol. Lett. **18,** 1013 (2006).
17. A. G. Kuznetsov, E. V. Podivilov, and S. A. Babin, J. Opt. Soc. Am. B **29,** 1231 (2012).